Resonance Current Suppression for AC-DC Active-Clamp Flyback Converter by Triangular Current Mode

Yasuo Uchida
Electrical, Electronics, and Information Engineering
Nagaoka University of Technology
Niigata, Japan
s203126@stn.nagaokaut.ac.jp

Hiroki Watanabe
Electrical, Electronics, and Information Engineering
Nagaoka University of Technology
Niigata, Japan
hwatanabe@vos.nagaokaut.ac.jp

Jun-ichi Itoh
Electrical, Electronics, and Information Engineering
Nagaoka University of Technology
Niigata, Japan
itoh@vos.nagaokaut.ac.jp

***Abstract*—This paper proposes the conduction loss reduction control method under Zero Voltage Switching (ZVS) operation of an AC-DC active-clamp flyback (ACF) converter for USB-Power Delivery. The proposed control method reduces the resonance current in the active clamp circuit by the reduction on-time of the clamp switch, while Triangular Current Mode control achieves ZVS to reduce the switching loss of the ACF converter. Moreover, the proposed control method provides the Power Factor Correction (PFC) capability without an additional PFC circuit because the proposed control method controls the input current by adjusting the on-time of the primary-side switch of the flyback converter. The detailed operation mode of both the conventional control method and the proposed control method is described. Experimental results of the 100-W active-clamp flyback converter demonstrate that the proposed method reduces the RMS current in the active-clamp circuit by 52.7% compared with the conventional control method.**

Keywords—Flyback converter, Triangular Current Mode, Zero Voltage Switching

I. Introduction

AC adapters and USB-Power Delivery (USB-PD) have been widely used for home appliance applications such as laptops and smartphones. A flyback converter is the popular circuit topology for their application because of its uncomplicated configuration, galvanic isolation between AC and low voltage DC side, and low cost. This application requires high-efficiency power conversion to have a high power density and extension of the power range of USB-PD.

For the high-efficiency power conversion, the control methods to achieve the soft switching for the flyback converter have been studied. The quasi-resonant (QR) control is the candidate of the soft-switching control method because it provides valley switching to reduce switching losses [1-6]. In the QR control, the drain-source voltage of the primary-side switch of the flyback converter fluctuates during the zero-current period by the resonance between the parasitic parameters and self-inductance of the transformer. The QR control ensures that the flyback converter achieves valley switching by adjusting the turn-on timing of the switching device to the valley of the drain-source voltage. However, the QR control does not achieve the complete ZVS because the input resonance parameters decide the valley voltage. As a result, the switching losses still occur.

Active-clamp flyback (ACF) converter achieves both ZVS and surge voltage suppression [7-12]. The ACF converter utilizes the resonance between the leakage inductance and the clamp capacitor to discharge the parasitic capacitor before turned-on of the semiconductor switch. However, the conduction and the copper losses increase due to the large resonance current.

The RMS current reduction method has been considered to reduce the conduction and the copper losses of the ACF converter [13]. This method uses two transformers and two secondary-side diodes with a parallel connection. However, this method requires additional components for the parallel connection.

This paper proposes the Triangular Current Mode (TCM) control for the ACF converter. The contribution of the paper is efficiency improvement owing to the reduction of the conduction and the copper losses. The proposed control method has a negative magnetizing-current period by adjusting the switching period of the secondary-side synchronous rectifier to discharge the parasitic capacitor. As a result, the ACF converter achieves ZVS without the resonance current in the active-clamp circuit. Moreover, the on-state of the clamp switch is set shorter than the one of the synchronous rectifier to reduce the resonance current.

This paper is organized as follows; First, the configuration of the ACF converter is shown. Secondly, the feature of the conventional control method is described, and the benefit of the proposed control method is described. Next, the on-state of the primary-side switch to achieve PFC is calculated. Finally, the fundamental operation and each evaluation are confirmed by experimental results.

II. Circuit Configuration

Fig. 1 shows the isolated AC-DC converter based on the ACF converter. The input side of the converter connects to the

AC voltage source, and the output side connects to the DC voltage source. This circuit consists of the synchronous rectifier and the ACF converter.

The synchronous rectifier improves the conversion efficiency because the on-resistance of the MOSFET is lower than the one of the diode. The synchronous rectifier switches synchronously with the grid frequency to full-wave rectify. In addition, The small capacitor is applied to the DC-link capacitor. Thus, the flyback converter controls the current of the AC voltage source to achieve Power Factor Correction (PFC) because the DC-link capacitor current is small, and the flyback converter provides isolation. In addition, The MOSFET is applied to the secondary side of the flyback converter to achieve the primary-side switch S_1 ZVS by conducting the negative-magnetizing current. The shunt resistor is applied to the secondary-side circuit to detect the magnetizing current i_{Lm}. The active-clamp circuit suppresses surge voltage.

III. Control Method

A. Conventional control method

Fig. 2 shows each waveform of the ACF converter with the conventional control method. The conventional control method discharges the parasitic capacitor of the primary-side switch C_{ds_S1} by the resonance current between the leakage inductance L_l and the clamp capacitor C_C to achieve ZVS for the primary-side switch S_1. This chapter describes the details of each mode.

<Mode 1>

In this mode, the primary-side switch S_1 turns on. The active-clamp switch S_C keeps off state. The input voltage v_{in} is applied to the leakage inductance L_l and the magnetizing inductance L_m of the transformer. The magnetizing current i_{Lm} linearly increases during this mode and flows into the primary side of the ACF converter.

<Mode 2>

This mode starts when the primary-side switch S_1 turns off. In this mode, the leakage current i_{Ll} continues to flow. The parasitic capacitor of the primary-side switch C_{ds_S1} is charged by the leakage current i_{Ll}. When charging the parasitic capacitor of the primary-side switch C_{ds_S1} is completed, the parallel diode of the clamp switch S_C and the secondary-side diode are turned on. The resonance current between the leakage inductance L_l and the clamp capacitor C_C occurs. In addition, the magnetizing current i_{Lm} flows into the secondary side of the ACF converter. Thus, the drain-source voltage of the clamp switch v_{ds_SC} decreases to 0 V because the leakage current i_{Ll} discharges the parasitic capacitor of the clamp switch C_{ds_SC}. In this mode, The magnetizing current i_{Lm} linearly decreases because the output voltage V_{out} is applied to the magnetizing inductance L_m of the transformer.

<Mode 3>

This mode starts when the clamp switch S_C turns on. In this mode, the clamp switch S_C achieves ZVS. The resonance current and the magnetizing current i_{Lm} continue to flow. When this mode is finished, the clamp capacitor current i_C is negative by the resonance current.

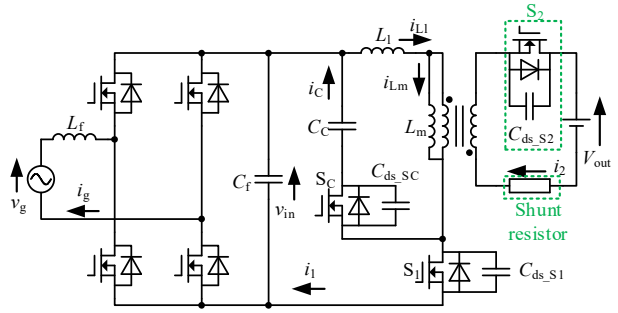

Fig. 1. Circuit configuration of AC-DC ACF converter.

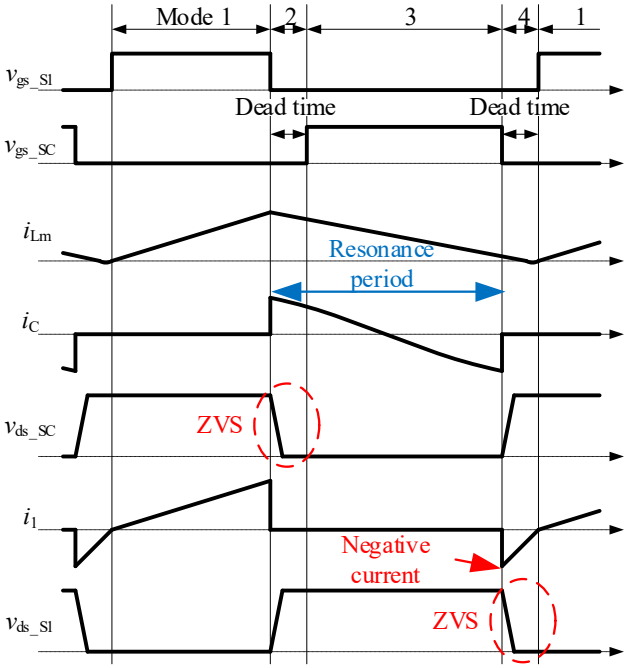

Fig. 2. Key waveforms of ACF converter with conventional control method. Primary-side switch S_1 achieves ZVS by resonance current. Clamp switch S_C also achieve ZVS.

<Mode 4>

This mode starts when the clamp switch S_C turns off. During this mode, the leakage current i_{Ll} continues to flow. The parasitic capacitor of the clamp switch C_{ds_SC} is charged by the leakage current i_{Ll}. When charging of the parasitic capacitor of the clamp switch C_{ds_SC} is completed, the parallel diode of the primary-side switch S_1 is turned on. Thus, the drain-source voltage of the primary-side switch v_{ds_S1} decreases to 0 V because the leakage current i_{Ll} discharges the parasitic capacitor of the primary-side switch C_{ds_S1}.

When next mode 1 starts, the primary-side switch S_1 achieves ZVS.

The conventional control method provides that all switches of the ACF converter achieve ZVS. However, the conduction and the copper losses increase due to the large resonance current between the leakage inductance L_l and the clamp capacitor C_C.

B. Proposed control method

Fig. 3 shows each waveform of the ACF converter with the proposed control method. The proposed control method discharges the parasitic capacitor of the primary-side switch C_{ds_S1} by the negative magnetizing current to achieve ZVS for the primary-side switch S_1. This chapter describes the details of each mode.

<Mode 1>

In this mode, the primary-side switch S_1 turns on for the time of the primary-side switch T_1. The secondary-side switch S_2 and the active-clamp switch S_C keeps off state. The input voltage v_{in} is applied to the leakage inductance L_l and the magnetizing inductance L_m of the transformer. The magnetizing current i_{Lm} linearly increases during this mode and flows into the primary side of the ACF converter.

<Mode 2>

This mode starts when the primary-side switch S_1 turns off. In this mode, the leakage current i_{Ll} continues to flow. The parasitic capacitor of the primary-side switch C_{ds_S1} is charged by the leakage current i_{Ll}. When charging the parasitic capacitor of the primary-side switch C_{ds_S1} is completed, the parallel diode of the secondary-side switch S_2 and the clamp switch S_C are turned on. The resonance current between the leakage inductance L_l and the clamp capacitor C_C occurs. Thus, the drain-source voltage of the clamp switch v_{ds_SC} decreases to 0 V because the resonance current discharges the parasitic capacitor of the clamp switch C_{ds_SC}. In addition, the magnetizing current i_{Lm} flows into the secondary side of the ACF converter. Thus, the drain-source voltage of the secondary-side switch v_{ds_S2} decreases to 0 V because the magnetizing current i_{Lm} discharges the parasitic capacitor of the secondary-side switch C_{ds_S2}. In this mode, The magnetizing current i_{Lm} linearly decreases because the output voltage V_{out} is applied to the magnetizing inductance L_m of the transformer.

<Mode 3>

This mode starts when the secondary-side switch S_2 turns on for the time of the secondary-side switch T_2, and the clamp switch S_C turns on for the time of the clamp switch T_C. In this mode, the secondary-side switch S_2 and the clamp switch S_C achieve ZVS. The resonance current and the magnetizing current i_{Lm} continue to flow. When this mode is finished, the clamp capacitor current i_C is negative by the resonance current.

<Mode 4>

This mode starts when the clamp switch S_C turns off. In this mode, The resonance current between the leakage inductance L_l and the clamp capacitor C_C does not flow. Thus, the proposed control method reduces the conduction time of the clamp switch S_C to reduce the RMS current of the clamp capacitor current i_C. The leakage current i_{Ll} continues to flow into the parallel diode of the primary-side switch S_1 until the leakage current i_{Ll} reaches 0 A. In addition, The magnetizing current i_{Lm} continues to flow into the secondary side of the ACF converter after the magnetizing current i_{Lm} crosses 0 A to achieve ZVS for the primary-side switch S_1. When the magnetizing current reaches the bottom, that is enough value to achieve ZVS for the primary-side switch S_1, this mode ends.

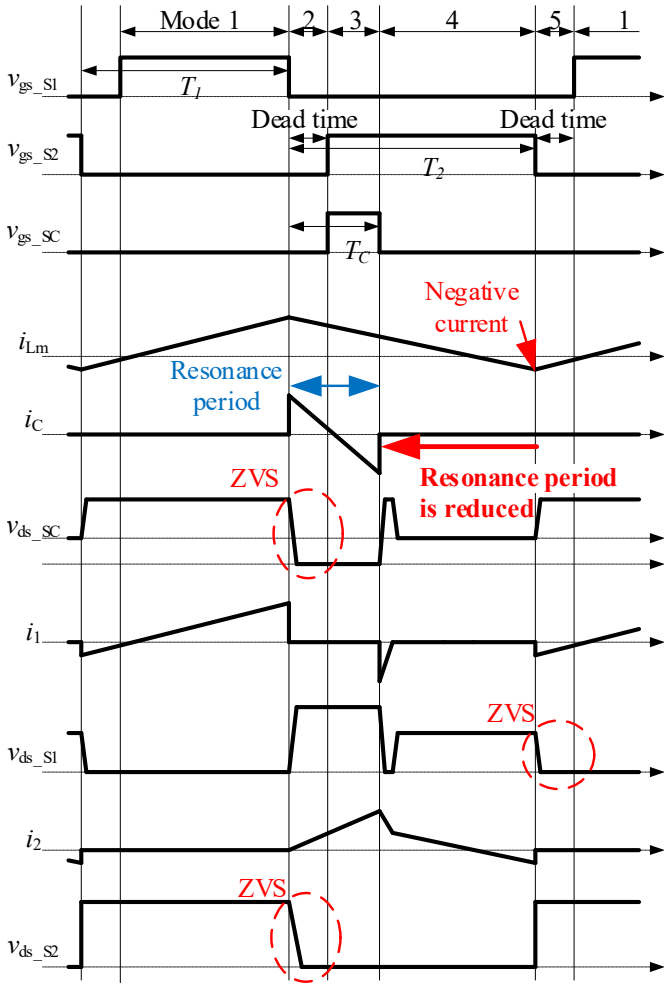

Fig. 3. Key waveforms of ACF converter with proposed control method. Primary-side switch S_1 achieves ZVS by negative magnetizing current. Secondary-side switch S_2 and active clamp switch S_C also achieve ZVS.

<Mode 5>

This mode starts when the secondary-side switch S_2 turns off. During this mode, the magnetizing current i_{Lm} continues to flow into the parallel diode of S_1. Thus, the drain-source voltage of the primary-side switch v_{ds_S1} decreases to 0 V because the magnetizing current i_{Lm} discharges the parasitic capacitor of the primary-side switch C_{ds_S1}.

When next mode 1 starts, the primary-side switch S_1 achieves ZVS.

The proposed control method provides that all ACF converter switches achieve ZVS. In addition, the proposed control method reduces the RMS current of the clamp capacitor current i_C by the reduction conduction time of the resonance current between the leakage inductance L_l and the clamp capacitor C_C.

C. Bottom current detection

Fig. 4 shows the magnetizing current i_{Lm} waveforms without parasitic parameters. According to Fig. 4, the magnetizing current i_{Lm} reaches the bottom while the magnetizing current i_{Lm} flows into the secondary side of the ACF converter. Thus, the proposed control method detects the secondary-side current i_2 by the shunt resistor.

Fig. 5 shows the zero-crossing detection circuit composed of the differential amplifier, buffer amplifier, LPF, Hysteresis comparator, and isolator. According to Fig. 5, the shunt resistor and the amplifier detect the secondary-side current i_2. After that, the hysteresis comparator detects the secondary-side current i_2 polarity. The ACF converter with the proposed control method requires isolation of the detected value of the secondary-side current i_2 because the primary side and the secondary side of the ACF converter are isolated. However, the propagation delay of isolation of analog detection value by an isolation amplifier is long. Thus, the proposed control method detects zero-crossing of the secondary-side current i_2.

The proposed control method estimates the secondary-side current based on the current drop time of the magnetizing current i_{Lm} from zero to bottom current I_{bot}. According to Fig. 4, the relationship between the current drop time T_{2bot} and the bottom current I_{bot} is expressed as

$$T_{2bot} = \frac{L_m}{NV_{out}} I_{bot} \tag{1}$$

where L_m is the magnetizing inductance of the transformer, V_{out} is the output voltage of the ACF converter, and N is the turn ratio of the transformer.

D. On-time calculation of the proposed control method

The proposed control method obtains the full-wave rectified average current of the primary-side current i_{1avg} to provide PFC. According to Fig. 4, the average primary-side current i_{1avg} is expressed as

$$i_{1avg}(t) = \frac{1}{2T_{sw}}\left(I_{peak} \times (T_1 - T_{1bot}) - I_{bot} T_{1bot}\right) \tag{2}$$

where T_{sw} is the switching period, I_{peak} is the peak of the magnetizing current, T_1 is the time of the primary-side switch, T_{1bot} is the reset time of the magnetizing current from the bottom current to zero. In addition, T_{1bot}, T_{sw}, and I_{peak} are expressed as

$$T_{1bot} = \frac{L_m}{|v_{in}(t)|} I_{bot} \tag{3}$$

$$T_{sw} = \frac{|v_{in}(t)| + NV_{out}}{NV_{out}} T_1 \tag{4}$$

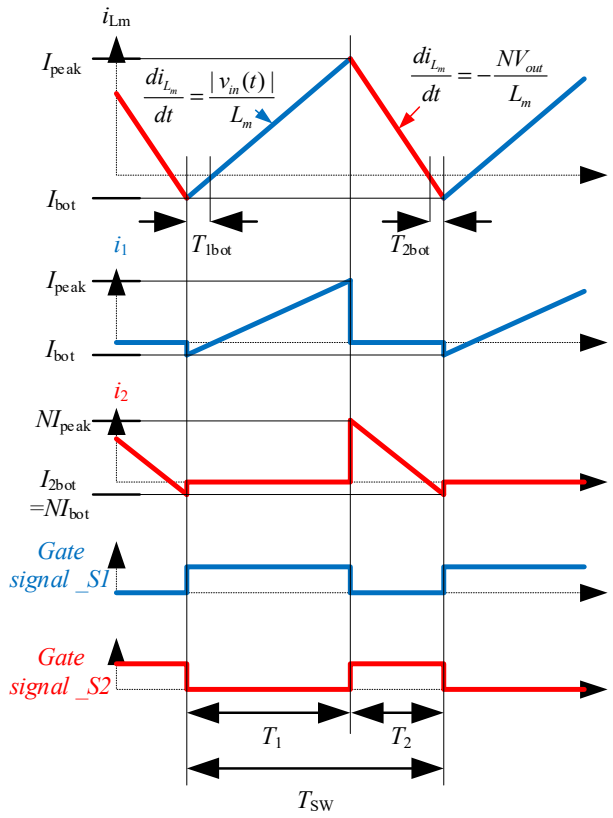

Fig. 4. Waveforms of Magnetizing current of flyback converter.

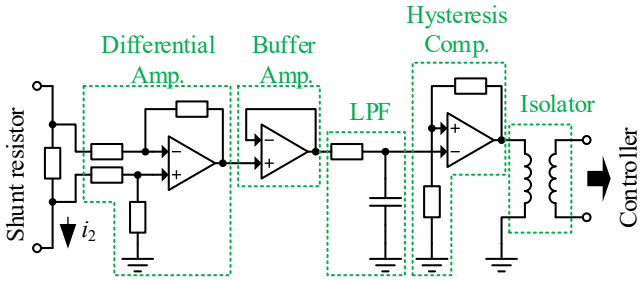

Fig. 5. Circuit configuration of zero-crossing detection circuit. This circuit detects zero-crossing of magnetizing current to control bottom current I_{bot}.

$$I_{peak} = \frac{|v_{in}(t)|}{L_m} T_1 - I_{bot} \tag{5}$$

where v_{in} is the input voltage. According to (2) ~ (5), the ratio of the average current of the primary-side current to the input voltage K_{iin}(t) is expressed as

$$K_{iin}(t) = \frac{i_{1avg}}{|v_{in}(t)|} = \frac{NV_{out}\left(T_1 - 2I_{bot}L_m \frac{1}{|v_{in}(t)|}\right)}{2L_m\left(|v_{in}(t)| + NV_{out}\right)} \tag{6}$$

K_{iin}(t) is constant in order to provide PFC. The following equation expresses K_{iin}(t), assuming the input power P and the RMS input voltage V_{in}.

$$K_{iin}(t) = \frac{P}{V_{in}^{\ 2}} \tag{7}$$

According to (6) and (7), at the time of the primary-side switch T_1 is expressed as

$$T_1 = \frac{2PL_m(|v_{in}(t)| + NV_{out})}{NV_{out}V_{in}^{\ 2}} + 2I_{bot}L_m\frac{1}{|v_{in}(t)|} \tag{8}$$

According to the slope of the magnetizing current i_{Lm}, the time of the secondary-side switch, T_2 is expressed as

$$T_2 = \frac{|v_{in}(t)|}{NV_{out}}T_1 \tag{9}$$

Finally, at the time of the clamp switch, T_C is expressed as

$$T_C = a \times \frac{|v_{in}(t)|}{NV_{out}}T_1 \tag{10}$$

where a is the ratio of the on-time of the clamp switch to the one of the secondary-side switches. a is typically between 0.0 and 1.0 depending on the drain-source voltage allowance of the switches because the drain-source voltage of the primary-side switch v_{ds_S1} and the clamp switch v_{ds_SC} increase due to reduce discharging time of the clamp capacitor C_C when a is small. On the other hand, the reduction of the RMS current in the active clamp circuit is expected. The optimization of the a will be considered for the reduction of the conduction loss in another paper.

IV. Experimental Results

Table 1 shows experimental parameters. This chapter shows experimental results using Fig. 1 to confirm ZVS and PFC. Note that, the AC voltage source is applied to the input side, and the DC voltage source is applied to the output side. In addition, the ratio of the on-time of the clamp switch to the one of the secondary-side switch a is 0.2. The prototype circuit demonstrates the validity of the proposed control method.

Fig. 6 shows the input waveforms of the ACF converter with the proposed control method. According to Fig 7, the proposed control method provides high-power factor operation. The sinusoidal input current THD is obtained as an experimental result at 5.46%.

Fig. 7 shows each waveform of the ACF converter with the proposed control method when the primary-side switch S_1 turns on under the condition that the grid voltage is the peak value. According to Fig. 7, the primary-side switch of the ACF converter achieves ZVS by the negative primary-side current i_1.

Table 1: Experimental parameters.

Symbol	Quantity	Value
f_{sw}	Switching frequency	30kHz ~ 60kHz
P_{out}	Output power	100 W
V_{in}	Input voltage	100 V
V_{out}	Output voltage	24 V
L_m	Magnetizing inductance	306 μH
L_l	Leakage inductance	24.7 μH
N	Turns ratio	5
C_C	Clamp capacitor	2.0 μF
L_f	Filter inductance	2.13 mH
C_f	Filter capacitor	440 nF

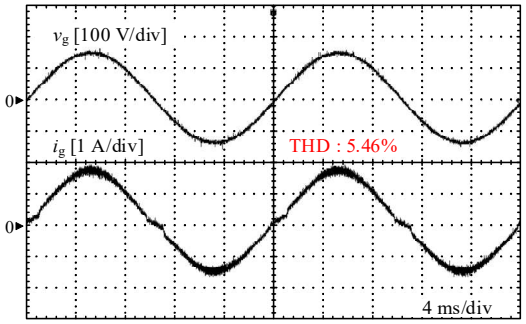

Figure 6: Input wavefoms of ACF converter with proposed control method. the proposed control method provides PFC.

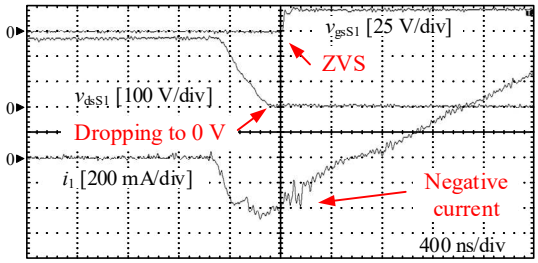

Fig. 7. Switching waveforms of primary-side switch S_1 of ACF converter with proposed control method. ZVS is achieved by TCM control.

Fig. 8 shows each current waveform when the input voltage v_{in} is 100 Vdc. Fig. 8(a) shows the current waveforms of the ACF converter with the conventional control method. According to Fig. 8(a), its resonance current continues to flow while the secondary-side current i_2 flows. Fig. 8(b) shows the current waveforms of the ACF converter with the proposed control method. According to Fig. 8(b), the conduction time of the clamp capacitor current i_C of the proposed control method is shorter than that of the conventional control method. As experimental results, the proposed control method reduces the RMS current of the clamp capacitor current i_C by 52.7%.

Fig. 9 shows the conduction loss of each switch of the ACF converter. The conduction loss is calculated from the RMS current and the on-resistance of the switches referred to in the datasheet. According to Fig. 9, the proposed control method

reduces the total conduction loss by 5.60%. In the flyback converter, A switch with small on-resistance is applied to the secondary-side switch S_2 because the drain-source voltage of the secondary-side switch v_{ds_S2} is lower than the one of the primary-side switch v_{ds_S1} and the clamp switch v_{ds_SC}. Thus, the reduction in the total conduction loss is improved because the on-resistance of the clamp switch S_C, which large RMS current flows, is small.

V. Conclusion

This paper discussed the control method for a flyback converter to reduce the conduction and the copper losses under ZVS operation. The proposed control method reduces the RMS current by decreasing the conduction time of the active-clamp circuit, and the switches of the ACF converter achieve ZVS by TCM control. In addition, the proposed control method provides PFC. As experimental results, the proposed control method provides that the AC-DC ACF converter achieves PFC, the switches achieve ZVS, and the RMS current of the clamp capacitor current i_C is reduced by 52.7%. In future work, the TCM control without a shunt resistor will be considered in order to implement of the efficiency.

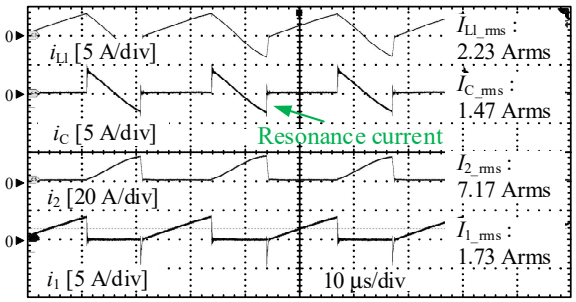

(a) With conventional control method.

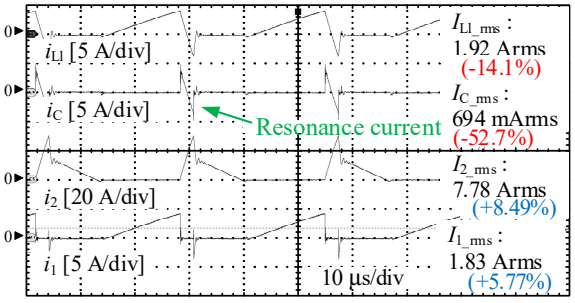

(b) With proposed control method.

Figure 8: Current wavefoms of ACF converter. The proposed control method reduces conduction time of resonance current. It reduced RMS current of i_C by 52.7%.

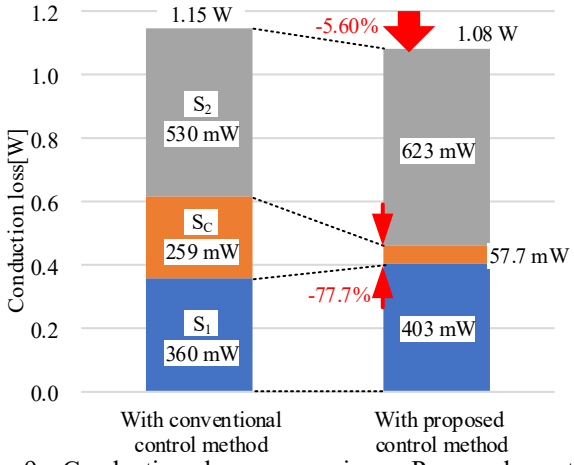

Fig. 9. Conduction loss comparison. Proposed control method reduces the total conduction loss by 5.60%.

References

[1] C. Wang, S. Xu, W. Shen, S. Lu and W. Sun, "A Single-Switched High-Switching-Frequency Quasi-Resonant Flyback Converter," IEEE Transactions on Power Electronics, vol. 34, no. 9, pp. 8785-8786, Sep. 2019.

[2] J. Zhang, H. Zeng, and X. Wu, "An Adaptive Blanking Time Control Scheme for an Audible Noise-Free Quasi-Resonant Flyback Converter," IEEE Transactions on Power Electronics, vol. 26, no. 10, pp. 2735-2742, Oct. 2011.

[3] X. Wu, Z. Wang and J. Zhang, "Design Considerations for Dual-Output Quasi-Resonant Flyback LED Driver With Current-Sharing Transformer," IEEE Transactions on Power Electronics, vol. 28, no. 10, pp. 4820-4830, Dec. 2012.

[4] C. Zhao, X. Xie, H. Dong and S. Liu, "Improved Synchronous Rectifier Driving Strategy for Primary-Side Regulated (PSR) Flyback Converter in Light-Load Mode," IEEE Transactions on Power Electronics, vol. 29, no. 12, pp. 6506-6517, Dec. 2014.

[5] C-H. Min and J-I. Ha, "Inner Supply Data Transmission in Quasi-Resonant Flyback Converters for Li-Ion Battery Applications Using Multiplexing Mode," IEEE Transactions on Power Electronics, vol. 34, no. 1, pp. 64-73, Jan. 2019.

[6] Y-C. Kang, C-C. Chiu, M. Lin, C-P. Yeh, J-M. Lin and K-H. Chen, "Quasiresonant Control With aDynamicFrequency Selector and Constant Current Startup Technique for 92% Peak Efficiency and 85% Light-Load Efficiency Flyback Converter," IEEE Transactions on Power Electronics, vol. 29, no. 9, pp. 4959-4969, Sep. 2014.

[7] R. Watson, F.C. Lee and G.C. Hua, "Utilization of an active-clamp circuit to achieve soft switching in flyback converters," IEEE Transactions on Power Electronics, vol. 11, no. 1, pp. 162-169, Jan. 1996.

[8] W. Meng, L. Li and F. Zhang, "Soft-switching Resonant Active Clamp Flyback Converter based-on GaN HEMTs for MHz High Step-up Applications," in 2021 IEEE Workshop on Wide Bandgap Power Devices and Applications in Asia, 2021, pp. 57-62.

[9] F-Z. Lin, T-J. Liang, K-H. Chen and K-F. Liao, "Primary-Side-Controlled AC-DC Single-Stage Active Clamp Flyback Converter," in 2023 IEEE Energy Conversion Congress and Exposition, 1997, pp. 3407-3414.

[10] Y. Yao, C. Wang, D. Sun and C. Sheng, "A High Precision PSR Constant Voltage Control Method for Active-Clamp Flyback Converter," IEEE Transactions on Industrial Electronics, (early access).

[11] Y. -M. Liu and L. -K. Chang, "Single-Stage Soft-Switching AC–DC Converter With Input-Current Shaping for Universal Line Applications," IEEE Transactions on Industrial Electronics, vol. 56, no. 2, pp. 467-479, Feb. 2009

[12] L, Xue and J. Zhang, "Highly Efficient Secondary-Resonant Active Clamp Flyback Converter," IEEE Transactions on Industrial Electronics, vol. 65, no. 2, pp. 1235-1243, Feb. 2018.

[13] Y-K, Lo and J-Y. Lin, "Active-Clamping ZVS Flyback Converter Employing Two Transformers," IEEE Transactions on Power Electronics, vol. 22, no. 6, pp. 2416-2423, Nov. 2007.